

Journal of Materials Chemistry A

Accepted Manuscript



This is an *Accepted Manuscript*, which has been through the Royal Society of Chemistry peer review process and has been accepted for publication.

Accepted Manuscripts are published online shortly after acceptance, before technical editing, formatting and proof reading. Using this free service, authors can make their results available to the community, in citable form, before we publish the edited article. We will replace this *Accepted Manuscript* with the edited and formatted *Advance Article* as soon as it is available.

You can find more information about *Accepted Manuscripts* in the [Information for Authors](#).

Please note that technical editing may introduce minor changes to the text and/or graphics, which may alter content. The journal's standard [Terms & Conditions](#) and the [Ethical guidelines](#) still apply. In no event shall the Royal Society of Chemistry be held responsible for any errors or omissions in this *Accepted Manuscript* or any consequences arising from the use of any information it contains.

Inkjet Printing of Conductive Patterns and Supercapacitors Using Multi-Walled Carbon Nanotubes/Ag Nanoparticles Based Ink

Siliang Wang,^a Nishuang Liu,^{*a} Jiayou Tao,^a Congxing Yang,^a Weijie Liu,^a Yuling Shi,^a Yumei Wang,^a Jun Su,^a Luying Li,^a and Yihua Gao^{*ab}

A multi-walled carbon nanotubes (MWCNTs) and silver (Ag) nanoparticles ink for inkjet printing was prepared by dispersing MWCNTs and Ag nanoparticles in water with the assistance of sodium dodecylbenzenesulfonate (SDBS). Highly conductive patterns of Ag-MWCNT were printed on paper by HP Deskjet 1010 inkjet printer. The patterns showed good stability during bending test and the low sheet resistance of $\sim 300 \Omega \text{ sq}^{-1}$ after being printed for 50 times. By simply adding manganese dioxide (MnO_2) nanoparticles with the diameter of 60-90 nm into the ink solution, patterned positive electrodes were prepared for asymmetric supercapacitors (ASCs) with filtrated MWCNT negative electrodes. The ASCs have a wide operation potential window of 1.8 V and excellent electrochemical performances, e.g. a high energy density of 1.28 mWh cm^{-3} at a power density of 96 mW cm^{-3} , a high retained ratio $\sim 96.9\%$ of its initial capacitance after 3000 cycles. The inkjet-printing acting as a simple, low-cost, non-contact deposition method can be fully integrated with the fabrication process in current printed electronics and has potential applications for energy storage.

Introduction

Technology advances in flexible and wearable/stretchable electronics such as flexible displays,¹ flexible and conformal antenna arrays,² electric circuits and chemical sensor,³ electronic solar cell arrays,⁴ radio frequency identification tags,⁵ microstructure electrochemical capacitors⁶ and so on, have promoted the demand for high-performance flexible conductive patterns.

Usually, in the fabrication of conductive patterns of flexible electronics,⁷⁻⁹ widely used photolithography involves many steps such as etching, electroplating *etc.* and is consuming, complicated and expensive. Compared with photolithography, inkjet printing is not only a easy access and cheap cost non-contact deposition method for obtaining conductive patterns, but also allows us to readily control the pattern geometry, location, electrical conductivity, film thickness and the uniformity of the film.¹⁰ Apart from conductive patterns, inkjet printing has many applications, such as thin-film transistors,¹¹⁻¹⁴ light-emitting devices,¹⁵ solar cells,^{16, 17} memory and magnetic application,^{18, 19} sensor and detectors,^{20, 21} and so on. However there have been few reports^{22, 23} on the production of energy storage devices *via* inkjet printing currently, and the present work addresses this key application. CNTs have become attractive nanoscale materials in various applications due to their unique properties. CNTs have highly accessible surface area, both high electrical conductivity and mechanical flexibility as well as high stability and low cost,²⁴ so CNTs are a promising materials for supercapacitors and an alternative for conductive electrodes. Nowadays, many researches are dedicated to conductive patterns by inkjet printing of CNTs.²⁵⁻²⁸ But the resistance of printed CNTs on flexible substrate was too high to be widely used in optoelectronic devices. Both Ag nanowire and sintered Ag nanoparticles have the properties of high conductivity,^{29, 30} but Ag nanoparticles is easier to be printed without clogging the nozzle. Mixing Ag nanoparticles with graphene could dramatically decrease the sheet resistance,³¹ so the mixture of Ag nanoparticles and CNTs may also decrease the sheet resistance without the change of mechanical flexibility.

Due to their high specific capacitance than carbon materials, transition metal oxides have been extensively studied in the past decades.³²⁻³⁵ MnO_2 is the most thoroughly investigated in supercapacitor applications because of its remarkable

theoretical specific capacitance (1370 F g^{-1}), nature abundance, low cost and environment-friendliness.³⁶⁻³⁸ Being limited by its poor electrical conductivity, MnO_2 has rarely achieved the theoretical specific capacitance in experiment.³⁹ The incorporation of MnO_2 with flexible conductive CNTs network can provide a feasible approach to overcome the above limitations. However, according to the equation: $E=0.5 \text{ CV}^2$ (C is specific capacitance; V is cell voltage), MnO_2 would compromise the specific energy density because of its narrow electrochemical working voltage window (0.8-1.0 V). This challenge could be addressed by fabricating ASCs that consist of two different electrodes,^{40, 41} *i.e.* MnO_2 -Ag-MWCNTs as the anode and filtered MWCNTs as the cathode. In this work, we demonstrate the fabrication of conductive patterns by inkjet printing Ag-MWCNT ink. Following that, ASCs were made by assembling the above mentioned MnO_2 -Ag-MWCNT anodes and filtered MWCNT cathodes. The ASCs show a wide operation potential window of 1.8 V and excellent electrochemical performance, *e.g.* a high energy density of 1.28 mWh cm^{-3} at a power density of 96 mW cm^{-3} , a high retained ratio $\sim 96.9\%$ of its initial capacitance after 3000 cycles.

Experimental Details

Ag-MWCNT and MnO_2 -Ag-MWCNT ink production

For the Ag-MWCNT ink production, 200 mg MWCNTs power (Beijing Boyu Gaoke New Material Technology Co., Ltd), 160 mg Ag nanoparticles (diameter of 20-120 nm, Shanghai Chaowei Nanotechnology Co., Ltd), 200 mg SDBS surfactant and 40 ml distilled water were added to a glass bottle. The mixture was stirred for 30 min to form uniform solution at room temperature and then probe ultrasonicated for 30 min. Afterwards, the Ag-MWCNT ink was obtained. For the MnO_2 -Ag-MWCNT ink production, the MnO_2 nanoparticles (60-90 nm) were synthesized similar to the literature.⁴² Typically, 50 mg KMnO_4 was dissolved in 30 ml de-ionized water, and then 1 ml ethanol was drop-wise added in under stirring. The addition of alcohol led to the formation of brownish precipitate of MnO_2 . After ethanol reduction, the mixtures were continually stirred for 24 h and then precipitates were filtered, washed with de-ionized water and

alcohol and dried at 60 °C for 24 h. The prepared MnO₂ nanoparticles, 200 mg MWCNTs powder, 160 mg Ag nanoparticles, 200 mg SDBS surfactant and 40 ml distilled water are added into a glass bottle, and the next procedure is similar to the preparation of the Ag-MWCNT ink.

Inkjet printing of Ag-MWCNT conductive patterns and MnO₂-Ag-MWCNT positive electrodes. Filtrating MWCNT negative electrodes

The Ag-MWCNT ink was injected into a clean ink cartridge (HP 1010) and printed using an HP Deskjet 1010 inkjet printer. In order to deposit the largest number of MWCNTs, the printer settings were adjusted for the best print quality, which ejected the largest volume of ink onto the substrate. Patterns for inkjet printing were quickly and easily designed in Auto CAD. Printing of the Ag-MWCNT ink was performed on paper. The Ag-MWCNT ink was printed with different times to observe the relationship between sheet resistance and number of prints. MnO₂ nanoparticles were added into Ag-MWCNT ink and anode was printed in the same method as the above conductive patterns. Vacuum filtration method was used to fabricate the MWCNT film cathode. MWCNTs were added into 40 ml distilled water with different mass (18 mg, 20 mg, 25 mg). Then 20 mg SDBS used as surfactant was dissolved in above solution and then stirred for 30 min, at last 30 min probe ultrasonication was adopted to further form a uniform solution. The as-obtained solution was filtered through a membrane (450 nm pore size). The obtained filter cake was dried in room temperature for 24 h.

Assemble of MnO₂-Ag-MWCNT/MWCNT ASCs

An ASC with aqueous electrolyte was assembled using a piece of MnO₂-Ag-MWCNT (1×1 cm²) and a piece of MWCNT film (1×1 cm²), with an electrolyte-soaked (4 M LiCl) separator in between. Adhesive tape was used to seal the ASCs.

Characterization

The morphologies and elements of printed conductive patterns were observed and analyzed with a scanning electron microscope (SEM, FEI Nova Nano-SEM 450). The XRD patterns of the samples were recorded with X-ray diffraction (XRD, PANalytical B.V. X'PertPRO). To investigate the flexibility of the electrodes, a three-dimensional (3D) mechanical stage was used to apply a strain on the free end of the sample, with the other end fixed tightly on a manipulation holder. The compressing process was illustrated in Supporting Figure S1. The different slope of the I-V curves which means the resistance of conductive films corresponds to different external compressive strain. Electrochemical measurements including galvanostatic charge/discharge (GCD) curves, cyclic voltammetry (CV) curves, electrochemical impedance spectroscopy (EIS, 100 KHz-0.01Hz) were conducted on an electrochemical workstation (CHI 660E). The electrochemical performance of individual electrodes was tested using three-electrode system with a 4 M LiCl solution serving as electrolyte, platinum electrode and Ag/AgCl were used as counter electrode and reference electrode prior to the fabrication of ASCs, respectively. The performance of ASCs was measured using a two-electrode configuration.

Results and Discussion

The fabrication of conductive patterns and patterned anodes was illustrated in Figure 1a. A personal computer was used to design conductive patterns which were then inkjet-printed by a home printer. The concentration of the ink is important for inkjet printing, because too high concentration will clog the nozzle, and too low concentration will increase the printing times to acquire the appropriate electrodes. For this reason, 5 mg ml⁻¹ MWCNTs, 4 mg ml⁻¹ Ag were chosen for the printed ink. The photos of ink were shown in Figure 1b. The mixtures

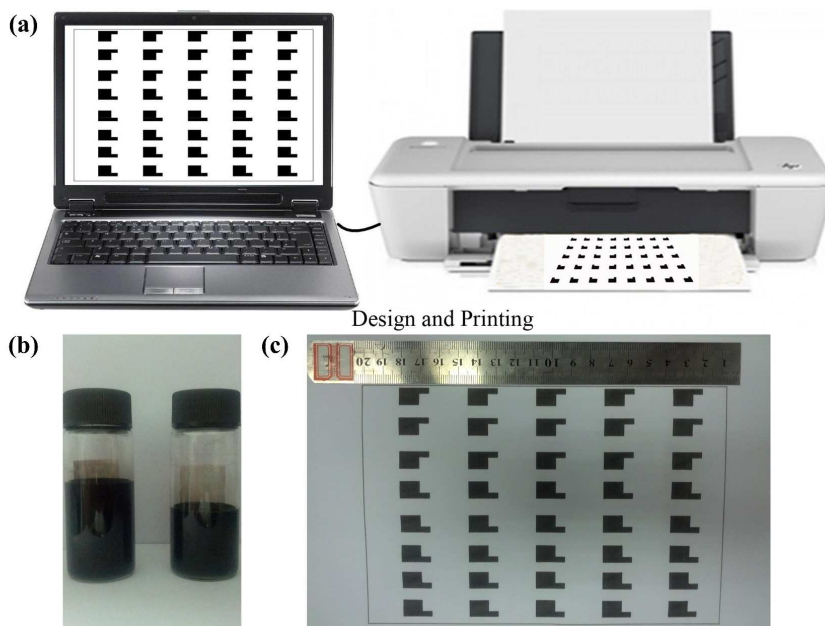


Figure 1 Overview of the fabrication process for inkjet-printing: (a) Design using a personal computer and inkjet-printing using a home printer. (b) The well-dispersed ink for inkjet-printing. (c) A Photo of patterned electrodes.

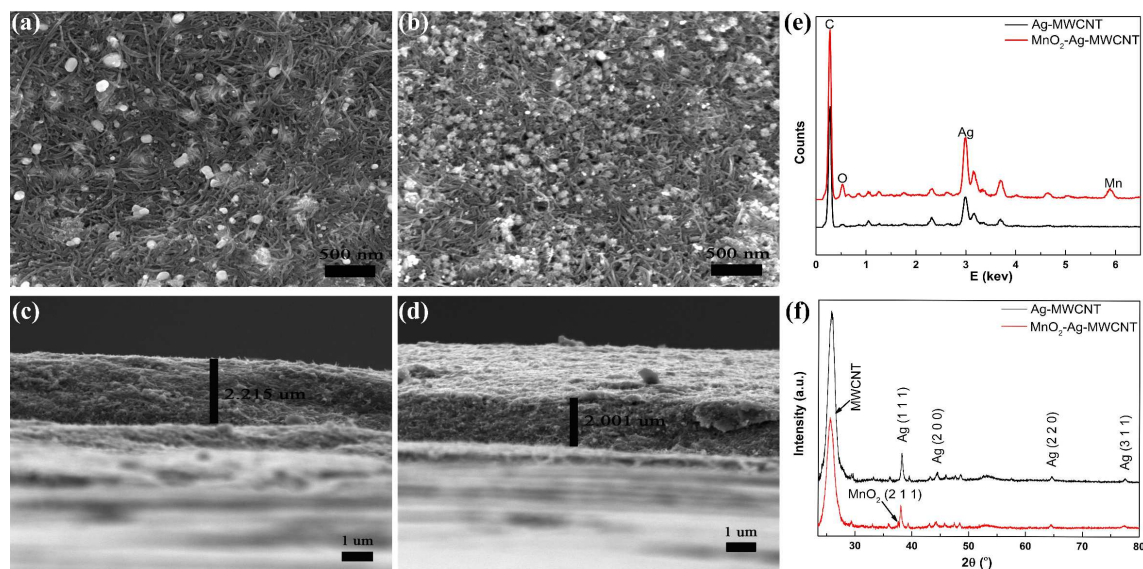


Figure 2 SEM images of (a) printed Ag-MWCNT conductive pattern and (b) printed MnO₂-Ag-MWCNT patterned positive electrode, respectively. The side view of (c) Ag-MWCNT and (d) MnO₂-Ag-MWCNT on paper substrates. (e) EDS of printed Ag-MWCNT and MnO₂-Ag-MWCNT. (f) XRD patterns of Ag-MWCNT and MnO₂-Ag-MWCNT.

of the ink dispersed well, and there was no obvious precipitation presented after a long time. Figure 1c is the photograph of inkjet-printed conductive patterns.

The XRD patterns of the as-prepared samples were presented in Supporting Figure S2 a. The samples were poorly crystallized and a broad peak at 37.5° can be clearly observed. This can be ascribed as (2 1 1) diffraction peak of α -MnO₂ (ICDD-JCPDS Card No. 44-0141). The diameter of MnO₂ nanoparticles was 60-90 nm (in supporting Figure S2 b). The morphologies of patterned electrodes were advertised in Figure 2a and b. Ag and MnO₂ nanoparticles well-distributed around the MWCNTs and have a tight connection with MWCNTs. The ejected MWCNTs formed tangled, dense, and homogeneous networks and tightly located on paper fiber (supporting Figure S2 c and d). The thickness of the printed Ag-MWCNT conductive pattern and the MnO₂-Ag-MWCNT patterned anode were 2.215 μm and 2.001 μm that were indicated in Figure 2c and d, respectively. The filtrated MWCNTs for cathode were also tightly tangled, and the thickness was 12.05 μm (see supporting Figure S2 e and f). In order to confirm the ingredients of the Ag-MWCNT conductive patterns and MnO₂-Ag-MWCNT patterned anodes, EDX and XRD analysis were used, as shown in Figure 2e and f. EDS spectrum confirmed that the C, and Ag signals were from the Ag-MWCNT conductive patterns (black line) and Mn, increased peak of O came from the patterned anodes (red line). The other peak came from paper substrates (supporting Figure S3 a). XRD patterns showed the peaks of MWCNT at 26°, 38.1°, 44.3°, 64.5°, 77.4° were attributed to the diffraction of (111), (200), (220), (311) crystalline planes of face-centered structure of Ag (black line). The peak at 37.5° came from (211) of MnO₂ (red line), as shown clearly in supporting Figure S3 b. Other peaks came from paper substrates (supporting Figure S3 c).

Both Ag-MWCNT ink and MWCNT ink were used to inkjet conductive patterns. The electrical resistance was rapidly reduced with the increasing number of overprinting. It was

also observed that adding Ag nanoparticles will significantly improve the conductivity (Figure 3a), which is mainly due to good conductivity of Ag nanoparticles and well-connection between Ag and MWCNTs. After being printed for 50 times, the conductive pattern fabricated by Ag-MWCNT ink reaches a sheet resistance as low as 300 Ω sq⁻¹, which is much lower than those reported in literatures.^{43, 44} For further characterizing the stability, we defined curvature as the bended chord height of total length divided by the total length ($C=H/L$, see Figure 3b inset). Figure 3b shows the changes in sheet resistance expressed as $(R-R_0)/R_0$, where R_0 is the initial sheet resistance and R is the sheet resistance after bending as a function of curvature. During bending, the changes of sheet resistance were random mainly due to the random connection between Ag and MWCNTs. However, the changes did not exceed 25% all the time. After we bend the electrode with a 20% curvature for 2000 times, the changes of sheet resistance were no more than 10% (Figure 3c). The inset demonstrated a foldable electric circuit by operating a LED on paper with Ag-MWCNT electrode. The conductive patterns may have potential applications for flexible/foldable optoelectronic devices.

To explore the potential applications in energy storage, the as-printed Ag-MWCNT electrode (mass density of 0.738 mg cm⁻²) and MnO₂-Ag-MWCNT electrode (mass density of 1.218 mg cm⁻²) were characterized with CV, GCD and EIS measurements. Figure 4a and b present CV curves of the anodes with the scanning rates from 2 mV s⁻¹ to 1 V s⁻¹. As expected, the electrode showed ideal capacitive behavior with rectangular CV curves (Figure 4a). The electrodes contained MnO₂ exhibited substantially larger current density than Ag-MWCNT electrodes (Figure 4c) because MnO₂ is more electrochemically active than MWCNT. As shown in Figure 4d, the GCD performance was further tested. The charge-discharge time of MnO₂-Ag-MWCNT system was actually prolonged, by 328% compared to the Ag-MWCNT system at the same current of 0.1 mA, indicating the great enhancement

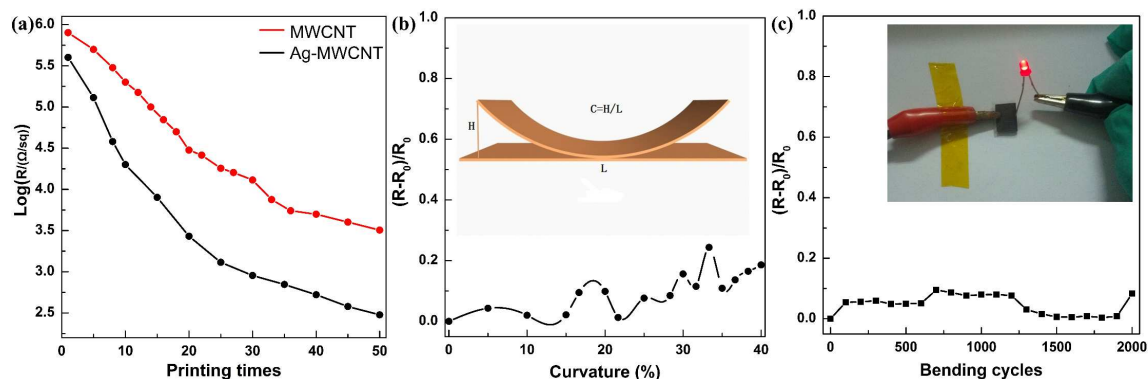


Figure 3 (a) Logarithm of sheet resistance versus number of prints. (b) Changes in the electrical resistance of conductive patterns vs curvature. (c) Changes in the electrical resistance of conductive patterns vs bending cycles, inset shows foldable circuit by operating a LED on paper with Ag-MWCNT electrode.

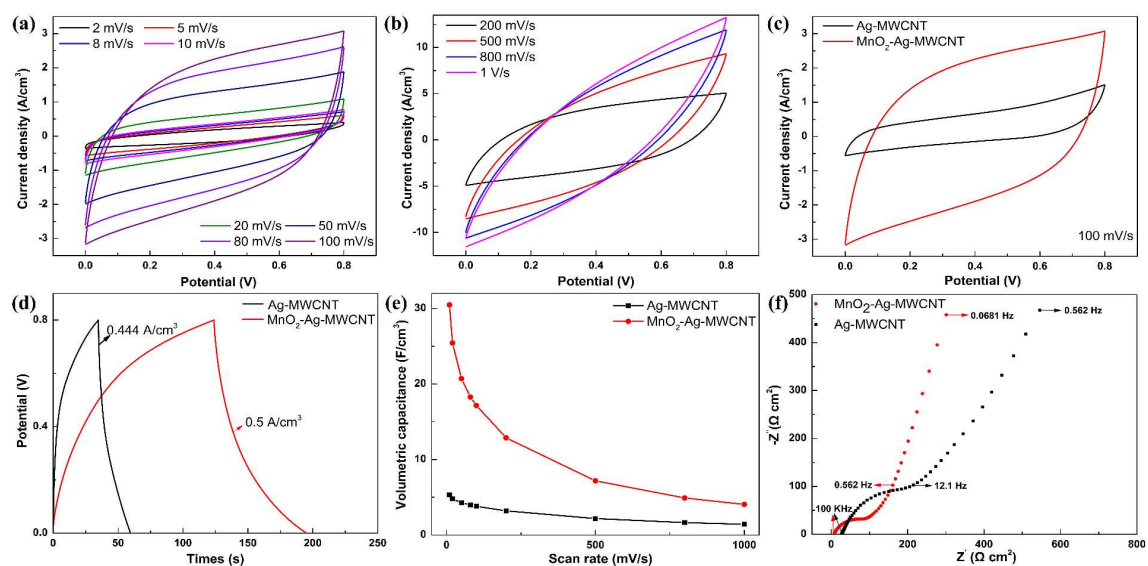


Figure 4 Electrochemical performance of the Ag-MWCNT and MnO₂-Ag-MWCNT electrodes. Cyclic voltammograms of the MnO₂-Ag-MWCNT electrodes with scan rate (a) from 0.001 V s⁻¹ to 0.1 V s⁻¹ and (b) from 0.2 V s⁻¹ to 1 V s⁻¹. (c) Cyclic voltammograms of the Ag-MWCNT and MnO₂-Ag-MWCNT electrodes at the scan rate of 0.1 V s⁻¹ (d) Galvanostatic charge discharge behavior of the electrodes with 0.444 A cm⁻², 0.5 A cm⁻², respectively. (e) Volumetric capacitance vs scan rate for the electrodes. (f) Nyquist plot of the electrodes.

in supercapacitance. The volumetric capacitance (see Figure 4e) was evaluated by the above CV results, which decreased with the scanning rate. At the scan rate of 10 mV s⁻¹, the volumetric capacitance of the MnO₂-Ag-MWCNT electrode was 30.5 F cm⁻³, about 5 times larger than that of the Ag-MWCNT electrode. Even at the scan rate of 1 V s⁻¹, the volumetric capacitance of the MnO₂-Ag-MWCNT electrode was 4.1 F cm⁻³. The EIS data were analyzed using Nyquist plot. The intercept of the plot at the X-axis represents the equivalent series resistance (ESR) of the electrode which determines the charge/discharge rate of the electrode.⁴⁵ Figure 4f shows the Nyquist plot of the electrodes, the ESR values of the Ag-MWCNT electrode (27.3 Ω) and the MnO₂-Ag-MWCNT electrode (8.1 Ω). The charge transfer resistances of Ag-MWCNT electrode and MnO₂-Ag-MWCNT electrode were 188.5 and 85.6 Ω, respectively (supporting Figure S4), which implied that adding MnO₂ nanoparticles would not increase the resistance of the electrodes. The densities of Ag-MWCNT electrode and MnO₂-Ag-MWCNT electrode were

0.333 and 0.609 g cm⁻³, respectively. Higher density means the tighter connections between different MWCNTs and Ag, and more beneficial for the electron transfer. It is well known that charge balance between positive and negative electrodes is crucial to maximize the energy density of ASCs.⁴⁶ So MWCNTs with different mass were filtrated. The capacitance of MWCNTs film with the mass density of 1.315 mg cm⁻² was the most closed to positive electrodes at the scanning rate of 100 mV s⁻¹ (supporting Figure S5 a). We chose the filtrated MWCNTs membranes (1.315 mg cm⁻²) to fabricate our cathodes. The cathodes showed ideal capacitive behaviour with rectangular and symmetry CV curves (supporting Figure S5 b). The volumetric capacitance reached 5.3 F cm⁻³ at the scanning rate of 10 mV s⁻¹ and the ESR was 16.5 Ω (supporting Figure S5 c and d).

To further investigate the performances of the asymmetric supercapacitor fabricated with inkjet-printed anode and well matched cathode, a variety of electrochemical measurements

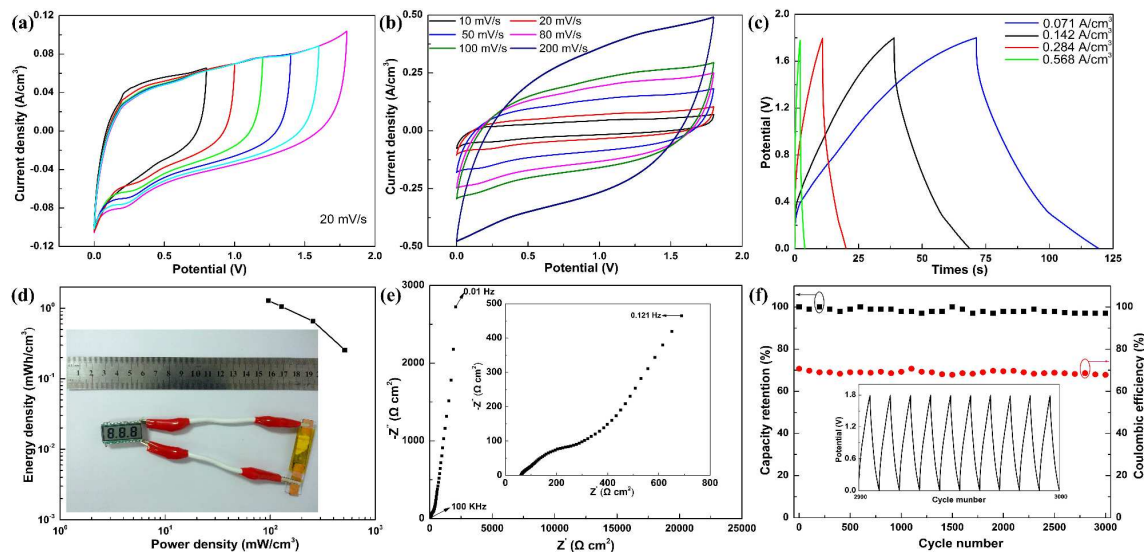


Figure 5 Electrochemical performances of the ASC. (a) CV curves of the device at different potential windows, the scan rate is 20 mV s^{-1} . (b) CV curves of the device at different scan rate. (c) Galvanostatic discharge curves of the device at different current density. (d) Energy and power density plot. (e) Nyquist plot. (f) Cycle life and Coulombic efficiency, inset shows the GCD curve from 2990^{th} to 3000^{th} .

have performed using two electrode configurations. The CV measurements indicated that the device exhibited a stable potential window up to 1.8 V (Figure 5a). The large potential window means a high energy density, which is a major advantage compared to common symmetric supercapacitor and a very important factor to meet the demand of application. As shown in Figure 5b, the asymmetric supercapacitor had well symmetrical and near rectangular CV curves at the potential window of 0–1.8 V, indicating that the device also had good capacitance performance. Good linear profiles of GCD curves with different current densities (Figure 5c) further confirm the perfect electrochemical behaviour of the device. The asymmetric supercapacitor showed high energy of 1.28 mWh cm^{-3} at a power density of 96 mW cm^{-3} . Moreover, a high power density of 512.1 mW cm^{-3} was obtained, and the energy density was still as high as $0.256 \text{ mWh cm}^{-3}$ at a discharge current density of 0.568 A cm^{-3} . A commercial liquid crystal display was successfully driven by the ASC after being fully charged (Figure 5d). Figure 5e presented the impedance spectrum of the as-fabricated device which exhibited a negligible 45° Warburg region and the ESR value (61.8Ω) of the device, indicating the fast ion transport at the active material-electrolyte interface. The impedance spectrum becomes almost a vertical line where the imaginary part of impedance increases dramatically in low frequency range, showing the perfect capacitive behaviour of ion diffusion in the electrode materials. GCD at the current density of 0.142 A cm^{-3} for 3000 cycles was carried out to evaluate the long-term cycle stability (as shown in Figure 5f). The capacitance only had a slight fluctuation in the whole process. The capacity retention is 96.9% after 3000 cycles and the Coulombic efficiency kept almost the same. This implied a good charge-discharge reversibility of the device.

Conclusions

Highly conductive patterns by inkjet-printing have been successfully prepared. By adding Ag nanoparticles to

MWCNT ink, the sheet resistance of the patterns decreased to $300 \Omega \text{ sq}^{-1}$ after being printed for 50 times. The conductive patterns could act as foldable electric circuit. MnO_2 -Ag-MWCNT anodes were also fabricated by inkjet printing. An asymmetric supercapacitor was fabricated by assembling an inkjet-printed MnO_2 -Ag-MWCNT anode with a filtrated MWCNT cathode. The supercapacitor has a wide operation potential window of 1.8 V and exhibits excellent electrochemical performance, e.g. a high density of 1.28 mWh cm^{-3} at a power density of 96 mW cm^{-3} , a high retained ratio $\sim 96.9\%$ of its initial capacitance after 3000 cycles. The inkjet-printing acting as a simple, low-cost, non-contact deposition method can be fully integrated with the fabrication process in current printed electronics and has potential applications for energy storage.

Acknowledgements

This work was supported by the National Basic Research program (2011CB933300) of China, the National Natural Science Foundation of China (11204093, 11374110), Overseas Master Program (MS2011HZKJ043), and the Fundamental Research Funds for the Central Universities (HUST: 2014TS124, 2013TS033). Y.H.G would like to thank Prof. Zhong-Lin Wang for the support of experimental facilities in WNLO of HUST.

Notes and references

^aCenter for Nanoscale Characterization & Devices (CNCD), Wuhan National Laboratory for Optoelectronics (WNLO) & School of Physics, Huazhong University of Science and Technology (HUST), Luoyu Road 1037, Wuhan 430074, China.
^bHubei Collaborative Innovation Center for Advanced Organic Chemical Materials, 368 Youyi Avenue, Wuhan 430062, China

1. Y. Chen, J. Au, P. Kazlas, A. Ritenour, H. Gates and M. McCreary, *Nature*, 2003, **423**, 136–136.

2. A. Rida, L. Yang, R. Vyas and M. M. Tentzeris, *Ieee Antennas And Propagation Magazine*, 2009, **51**, 13-23.
3. L. Huang, Y. Huang, J. J. Liang, X. J. Wan and Y. S. Chen, *Nano Research*, 2011, **4**, 675-684.
4. V. Marin, E. Holder, M. M. Wienk, E. Tekin, D. Kozodaev and U. S. Schubert, *Macromolecular Rapid Communications*, 2005, **26**, 319-324.
5. G. Orecchini, F. Alimenti, V. Palazzari, A. Rida, M. M. Tentzeris and L. Roselli, *Iet Microwaves Antennas & Propagation*, 2011, **5**, 993-1001.
6. D. Pech, M. Brunet, P. L. Taberna, P. Simon, N. Fabre, F. Mesnilgrente, V. Conedera and H. Durou, *Journal Of Power Sources*, 2010, **195**, 1266-1269.
7. J. G. Ok, M. K. Kwak, C. M. Huard, H. S. Youn and L. J. Guo, *Advanced materials*, 2013, **25**, 6554-6561.
8. B. Schumm, F. M. Wissler, G. Mondin, F. Hippauf, J. Fritsch, J. Grothe and S. Kaskel, *Journal Of Materials Chemistry C*, 2013, **1**, 638-645.
9. J. Jang, Y. Song, H. Oh, D. Yoo, D. Kim, H. Lee, S. Hong, J. K. Lee and T. Lee, *Applied Physics Letters*, 2014, **104**.
10. A. Chiolerio, M. Cotto, P. Pandolfi, P. Martino, V. Camarchia, M. Pirola and G. Ghione, *Microelectronic Engineering*, 2012, **97**, 8-15.
11. T. Shimoda, Y. Matsuki, M. Furusawa, T. Aoki, I. Yudasaka, H. Tanaka, H. Iwasawa, D. H. Wang, M. Miyasaka and Y. Takeuchi, *Nature*, 2006, **440**, 783-786.
12. Y. Y. Noh, X. Y. Cheng, H. Sirringhaus, J. I. Sohn, M. E. Welland and D. J. Kang, *Applied Physics Letters*, 2007, **91**.
13. M. B. Madec, P. J. Smith, A. Malandraki, N. Wang, J. G. Korvink and S. G. Yeates, *Journal Of Materials Chemistry*, 2010, **20**, 9155-9160.
14. D. H. Lee, S. Y. Han, G. S. Herman and C. H. Chang, *Journal Of Materials Chemistry*, 2009, **19**, 3135-3137.
15. G. Mauthner, K. Landfester, A. Kock, H. Bruckl, M. Kast, C. Stepper and E. J. W. List, *Organic Electronics*, 2008, **9**, 164-170.
16. D. Angmo, J. Sweelssen, R. Andriessen, Y. Galagan and F. C. Krebs, *Advanced Energy Materials*, 2013, **3**, 1230-1237.
17. Y. Y. Sun, Y. J. Zhang, Q. Liang, Y. Zhang, H. J. Chi, Y. Shi and D. N. Fang, *Rsc Advances*, 2013, **3**, 11925-11934.
18. W. Voit, W. Zapka, L. Belova and K. V. Rao, *Iee Proceedings-Science Measurement And Technology*, 2003, **150**, 252-256.
19. P. Tiberto, G. Barrera, F. Celegato, M. Coisson, A. Chiolerio, P. Martino, P. Pandolfi and P. Allia, *European Physical Journal B*, 2013, **86**.
20. E. Katzir, S. Yochelis, Y. Paltiel, S. Azoubel, A. Shimoni and S. Magdassi, *Sensors And Actuators B-Chemical*, 2014, **196**, 112-116.
21. X. Liu, L. L. Gu, Q. P. Zhang, J. Y. Wu, Y. Z. Long and Z. Y. Fan, *Nature communications*, 2014, **5**.
22. A. Chiolerio, S. Bocchini and S. Porro, *Advanced Functional Materials*, 2014, **24**, 3375-3383.
23. L. S. Fan, N. Q. Zhang and K. N. Sun, *Chemical Communications*, 2014, **50**, 6789-6792.
24. H. Pan, J. Y. Li and Y. P. Feng, *Nanoscale Research Letters*, 2010, **5**, 654-668.
25. J. W. Song, J. Kim, Y. H. Yoon, B. S. Choi, J. H. Kim and C. S. Han, *Nanotechnology*, 2008, **19**.
26. T. Kim, H. Song, J. Ha, S. Kim, D. Kim, S. Chung, J. Lee and Y. Hong, *Applied Physics Letters*, 2014, **104**.
27. R. P. Tortorich, E. Song and J. W. Choi, *Journal Of the Electrochemical Society*, 2014, **161**, B3044-B3048.
28. A. Shimoni, S. Azoubel and S. Magdassi, *Nanoscale*, 2014, **6**, 11084-11089.
29. L. B. Hu, H. S. Kim, J. Y. Lee, P. Peumans and Y. Cui, *Acs Nano*, 2010, **4**, 2955-2963.
30. A. Chiolerio, G. Maccioni, P. Martino, M. Cotto, P. Pandolfi, P. Rivolo, S. Ferrero and L. Scaltrito, *Microelectronic Engineering*, 2011, **88**, 2481-2483.
31. L. Li, Y. Guo, X. Zhang and Y. Song, *J. Mater. Chem. A*, 2014, **2**, 19095-19101.
32. Q. Li, Z. L. Wang, G. R. Li, R. Guo, L. X. Ding and Y. X. Tong, *Nano letters*, 2012, **12**, 3803-3807.
33. L. Y. Yuan, X. H. Lu, X. Xiao, T. Zhai, J. J. Dai, F. C. Zhang, B. Hu, X. Wang, L. Gong, J. Chen, C. G. Hu, Y. X. Tong, J. Zhou and Z. L. Wang, *Acs Nano*, 2012, **6**, 656-661.
34. X. Xiao, T. P. Ding, L. Y. Yuan, Y. Q. Shen, Q. Zhong, X. H. Zhang, Y. Z. Cao, B. Hu, T. Zhai, L. Gong, J. Chen, Y. X. Tong, J. Zhou and Z. L. Wang, *Advanced Energy Materials*, 2012, **2**, 1328-1332.
35. C. Guan, J. P. Liu, C. W. Cheng, H. X. Li, X. L. Li, W. W. Zhou, H. Zhang and H. J. Fan, *Energy & Environmental Science*, 2011, **4**, 4496-4499.
36. J. Y. Tao, N. S. Liu, W. Z. Ma, L. W. Ding, L. Y. Li, J. Su and Y. H. Gao, *Scientific Reports*, 2013, **3**.
37. J. Liu, L. Zhang, H. B. Wu, J. Lin, Z. Shen and X. W. Lou, *Energy Environ. Sci.*, 2014.
38. N. S. Liu, W. Z. Ma, J. Y. Tao, X. H. Zhang, J. Su, L. Y. Li, C. X. Yang, Y. H. Gao, D. Golberg and Y. Bando, *Advanced materials*, 2013, **25**, 4925-4931.
39. M. Toupin, T. Brousse and D. Belanger, *Chemistry Of Materials*, 2004, **16**, 3184-3190.
40. J. Yan, Z. J. Fan, W. Sun, G. Q. Ning, T. Wei, Q. Zhang, R. F. Zhang, L. J. Zhi and F. Wei, *Advanced Functional Materials*, 2012, **22**, 2632-2641.
41. X. Xiao, T. Li, Z. Peng, H. Jin, Q. Zhong, Q. Hu, B. Yao, Q. Luo, C. Zhang, L. Gong, J. Chen, Y. Gogotsi and J. Zhou, *Nano Energy*, 2014, **6**, 1-9.
42. R. Jiang, T. Huang, Y. Tang, J. Liu, L. Xue, J. Zhuang and A. Yu, *Electrochimica Acta*, 2009, **54**, 7173-7179.
43. K. Kordas, T. Mustonen, G. Toth, H. Jantunen, M. Lajunen, C. Soldano, S. Talapatra, S. Kar, R. Vajtai and P. M. Ajayan, *Small*, 2006, **2**, 1021-1025.
44. O.-S. Kwon, H. Kim, H. Ko, J. Lee, B. Lee, C.-H. Jung, J.-H. Choi and K. Shin, *Carbon*, 2013, **58**, 116-127.
45. M. D. Stoller, S. J. Park, Y. W. Zhu, J. H. An and R. S. Ruoff, *Nano letters*, 2008, **8**, 3498-3502.
46. J. P. Zheng, *Journal Of the Electrochemical Society*, 2003, **150**, A484-A492.



Inkjet printing of conductive Ag-MWCNT patterns and MnO₂-Ag-MWCNT anodes for supercapacitors.